Electrochimica Acta 297 (2019) 613–622

Contents lists available at ScienceDirect

Electrochimica Acta

journal homepage: www.elsevier.com/locate/electacta

Addition of reduced graphene oxide to an activated-carbon cathode increases electrical power generation of a microbial fuel cell by enhancing cathodic performance

Bonyoung Koo [a], Seung-Mok Lee [b], Sang-Eun Oh [c], Eun Jung Kim [d], Yuhoon Hwang [e], Dongjune Seo [f], Jin Young Kim [g], Yung Ho Kahng [g], Yong Woon Lee [a], Seon-Yong Chung [a], Seong-Jun Kim [a], Jeong Hun Park [a], Sokhee P. Jung [a, *]

[a] Department of Environment and Energy Engineering, Chonnam National University, Gwangju 61186, Republic of Korea
[b] Department of Environment Engineering, Catholic Kwandong University, Gangneung 25601, Republic of Korea
[c] Department of Biological Environment, Kangwon National University, Chuncheon, Gangwon-do 24341, Republic of Korea
[d] Department of Environmental Engineering, Mokpo National University, Jeollanam-do 58554, Republic of Korea
[e] Department of Environmental Engineering, Seoul National University of Science and Technology, Seoul 01811, Republic of Korea
[f] Research Institute of Biotechnology, CJ CheilJedang, Gyeonggi-do 16495, Republic of Korea
[g] Department of Physics Education, Chonnam National University, Gwangju 61186, Republic of Korea

ARTICLE INFO

Article history:
Received 3 July 2018
Received in revised form
27 November 2018
Accepted 3 December 2018
Available online 4 December 2018

Keywords:
Microbial fuel cell
Cathode
Catalyst layer
Activated carbon
Reduced graphene oxide
Impedance

ABSTRACT

Activated carbon (AC) is an inexpensive catalyst for oxygen reduction in an air cathode of microbial fuel cells (MFCs). In the AC-based cathode, carbon black (CB) is used as a conductive supporting material. In this study, it was hypothesized cathodic performance would increase if reduced graphene oxide (rGO) replaces CB in an optimum ratio. rGO replaced CB in the four different weight ratios of rGO toCB: 0:30 (rGO0); 5:25 (rGO5); 15:15 (rGO15); 30:0 (rGO30). Maximum power density was the best in rGO15 (2642 mW/m^2) followed by rGO5 (2142 mW/m^2). In the optimum external resistance operation, rGO5 and rGO15 showed similar power (~1060 mW/m^2), higher than the others. Linear sweep voltammetry, cyclic voltammetry, and impedance spectroscopy also showed that the optimal rGO additions improved cathodic performance and reduced cathodic internal resistance. Due to the flatter and wider shape of rGO and 5 times higher electrical conductivity than CB, the rGO addition improved the cathodic performance, but the complete replacement of CB with rGO decreased the cathodic performance due to the increased thickness and the morphological crack. The optimum rGO addition is a simple and effective method for improving cathodic performance.

1. Introduction

Microbial fuel cells (MFCs) are innovative bioelectrochemical systems (BES) that are being developed for an energy positive wastewater treatment process that generate electricity from the organic waste with the concurrent wastewater treatment [1–3]. In MFCs, exoelectrogenic biofilm on the anode decomposes organic matter and releases electrons, which move to the cathode through an external circuit, and an oxygen reduction reaction (ORR) occurs on the cathode catalysts.

Platinum (Pt) has been used as a typical cathode catalyst for the ORR in the MFCs, but its high price is a bottleneck for commercialization of MFCs. One of the most promising alternative catalysts for platinum is activated carbon (AC) powder [4,5]. AC has lower catalytic activity for oxygen reduction reaction than Pt, but AC (~$ 1.4 kg^{-1}) is very cheaper than platinum (~$ 69,000 kg^{-1}) [6]. Therefore, by loading much higher amount of AC powder (AC: 26.45 mg/cm^2) than Pt powder (Pt: 0.5 mg/cm^2), AC cathodes with similar performance to those of Pt cathodes have been fabricated [7,8].

Along with increasing a current collector area [9], various AC cathodes with a stainless steel mesh current collector have been tested to improve cathode performance (Table 1). Maximum power production increased by physical and chemical treatments of AC

* Corresponding author.
E-mail address: sokheejung@chonnam.ac.kr (S.P. Jung).

https://doi.org/10.1016/j.electacta.2018.12.024
0013-4686/

Table 1
Comparison of maximum power densities (p_{max}) of various MFC tests with various activated carbon based cathodes with a stainless steel mesh current collectors. The control cathode is non-treated one. A single chamber MFC was used as a reactor in the all the tests.

Cathode Fabrication (size)	AC Treatment	Anode	Medium Substrate Reactor Volume	p_{max} AC-cathode (mW/m^2)	p_{max} control (mW/m^2)	Increasing rate (%)	Polarization method	Ref.
Rolling-pressed (7 cm^2)	Strong alkaline (KOH 3 M)	AC-SS mesh	50 mM PBS 1 g/L Acetate 28 mL	957	804	19	ERC (30min, 9ExR)	[10]
Rolling-pressed (7 cm^2)	Strong Acidic (H_3PO_4, 1 M)	Carbon felt	WW + PBS 2 g/L Acetate 28 mL	1546	638	142	ERC (10min, 9ExR)	[11]
Hot-pressed (7 cm^2)	Fe-N-C framework	Carbon brush	50 mM PBS 1 g/L Acetate 28 mL	2600	1600	62	ERC (20min, 7ExR)	[12]
Hot-pressed (7 cm^2)	carbon black (10% ratio)	Carbon brush	50 mM PBS 1 g/L Acetate 28 mL	1560	1340	16	ERC (20min, 9ExR)	[16]
Hot-pressed (7 cm^2)	carbon black and heat treatment (800 °C, Ar)	Carbon brush	50 mM PBS 1 g/L Acetate 24 mL	1900	1610	18	ERC[a] (20min, 9ExR)	[17]
Hot-pressed (7 cm^2)	FeDTA and heat treatment (800 °C, Ar)	Carbon brush	50 mM PBS 1 g/L Acetate 28 mL	1410	1040	35	ERC (20min, 9ExR)	[13]
Circular pellet shape (2.85 cm^2)	Added Fe-aminoantipyrine	Carbon brush	WW + 0.1 M K-PB 3 g/L Acetate 125 mL	2170	1040	108	IV polarization (0.2 mV/s)	[14]
Circular pellet shape (2.85 cm^2)	Added Fe-Nicarbazin	Carbon brush	WW + 0.1 M K-PB 3 g/L Acetate 125 mL	1850	430	330	IV polarization (0.2 mV/s)	[15]
Circular pellet shape (2.85 cm^2)	Graphene nanosheets	Carbon brush	WW + 0.1 M K-PB 3 g/L Acetate 125 mL	2059	1017	102	IV polarization (0.2 mV/s)	[22]

[a] ERC: External resistance change method.

powder in the cathodes. Alkaline or acidic treatments of AC powder enhanced cathodic performance and MFC power generation by increasing effective surface area. Strong alkaline treatment (KOH) of AC powder increased maximum power density (p_{max}) (957 mW/m^2) by 19% compared to the plain AC cathode (804 mW/m^2) [10]. Strong phosphoric acidic treatment (H_3PO_4) of AC powder increased p_{max} (1546 mW/m^2) by 142% compared to the plain AC cathode (638 mW/m^2) [11]. Functional groups were attached to the AC surface to improve catalytic reaction and electrical conductivity. Attaching the Fe-N-C framework to the AC surface improved p_{max} (2600 mW/m^2) by 62% over the plain AC cathode (1600 mW/m^2) [12].

Addition of conductive material to a cathode is very a simple and easy way to enhance cathodic performance. When FeEDTA was added instead of CB, p_{max} (1410 mW/m^2) increased by 35% over the non-treated one (1040 mW/m^2) [13]. When the iron-aminoantipyrine (Fe-AAPyr) catalyst was added to a cathode, p_{max} (2170 mW/m^2) was 108% higher than that of the control cathode (1040 mW/m^2) [14]. When the metal structure (iron-nicarbazin) was added, p_{max} (1850 mW/m^2) was 330% higher than that of the plain AC cathode (430 mW/m^2) [15]. When carbon black (CB) was added to the AC cathode (CB:AC = 1:10) without reducing the total AC weight, p_{max} (1560 mW/m^2) improved by 16% over the control without carbon black (1340 mW/m^2) [16]. Additions of AC and CB particles pre-treated at 800 °C showed the highest p_{max} of 1900 mW/m^2, which is 18% higher than that of the non-treated control (1610 mW/m^2) [17].

Because graphene is a thin carbonaceous material with superb conductivity and chemical stability, graphene has gained substantial interests for various applications [18–20]. Among the graphene-like materials, graphene oxide have been used as an ideal carbon-based electrode material [21]. During the thermal reduction process of graphene oxide (GO), GO with a sheet form expands due to the thermal reduction of its oxygen constituents. Through this process, its conductivity and surface area increase. When rGO is added to the cathode catalyst layer, conductivity of the catalyst layer can increase. In a previous study, rGO particles were added as a cathodic catalyst to the AC cathode by replacing AC in three different ratios, and the 10 mg/cm^2 loading of rGO showed the highest p_{max} 2059 mW/m^2, which is 102% higher than the AC cathode (1017 mW/m^2) [22]. The rGO particles were used as an electrochemical reduction catalyst, and cathode performance was enhanced by replacing activated carbon.

In this study, it was hypothesized cathodic performance would increase if reduced graphene oxide (rGO) replaces CB in an optimum ratio. rGO was tested as an additive to the cathodic catalyst layer in the AC-based cathode. Because rGO has a high electrical conductivity and unique shape with flat and large area, it can be used for improving the electrical conductivity and facilitating electron transfer in the cathodic catalyst layer by intercalation into the catalyst layer in replace of CB [16]. The same amount of AC was used in all the cathodes, CB was replaced with rGO in the four different weight ratios, and these four types of cathodes were tested in the single chamber cubic MFC.

2. Materials and methods

2.1. Preparation of reduced graphene oxide

Graphene oxide powder (GO-V30-100, Standard Graphene Inc.,

South Korea) was thermally reduced at 300 °C for 5 min in a tube furnace (HTF-Q85, HAN tech, South Korea) flowing 4% H_2/Ar gas. After this reduction process, reduced graphene oxide (rGO) powder was obtained. The GO had 45–50% carbon, 45–50% hydrogen, less than 2% hydrogen and no nitrogen detected along with more than 7.0 μm of lateral size.

2.2. Characterizations of carbon materials

X-ray photoelectron spectroscopy (XPS) was performed to determine atomic compositions and functional groups of the rGO surface by using a surface analysis instrument (Multilab 2000, Thermo Fisher Inc., USA). rGO samples for XPS were prepared by spin-coating at 1500 rpm on Si_3N_4 (50 nm)/Si substrates to form a thin layer from a GO solution prepared at 0.1 wt% using N,N-Dimethylformamide solution. The rGO sample was thermally reduced before the measurements. The elemental and peak fitting analysis of C 1s (285 eV), N 1s (397 eV) and O 1s (532 eV) peak position.

Total carbon (C), hydrogen (H) and nitrogen (N) contents of GO and rGO samples were analyzed using an organic elemental analyzer (FLASH 2000, Thermo Scientific, USA). The thickness of rGO and GO samples was measured by atomic force microscope (AFM, Veeco, Multimode V, USA). For AFM measurement, 0.05% by weight of each sample was dispersed in an organic solvent (N-Methyl-2-pyrrolidone) by sonication for 20 min. One drop of each sample solution dispersed on the oxided surface treated silicon substrate was spin-coated using a spin coater. Spin coating was conducted at 500 rpm for 5 s, 800 rpm for 10 s, and 1000 rpm for 15 s. The lateral size was measured by FE-SEM (Zeiss, Sigma, Germany) and the thickness was measured by AFM (Veeco, Multimode V, USA).

To compare the morphological features of CB and rGO, another AFM (XE-100, Park Systems Inc., South Korea) was performed. The CB sample was also prepared in the same way as above. To compare the conductivities of CB and rGO, each sample was formed into a coin-shaped pellet by using a manual contact system (CMT-100s, Advanced Instrument Technology Co., South Korea) at 28 MPa, followed by the conductivity measurement.

2.3. Electrode fabrication

For a duplicate experiment, two cathodes for each condition were made under the same conditions. An air cathode was made with activated carbon (AC) as an oxygen reduction catalyst, stainless steel mesh as a current collector, and PVDF as an catalyst binder [6]. To prepare PVDF solution, PVDF powder (~53,400 Da; Sigma-Aldrich, USA) was added to N,N-dimethylacetamide (DMAc) in a ratio of 10% (w/v), and stirred at room temperature for 8 h with a magnetic stirring bar. The catalytic mixture consisted of 300 mg of AC powder (Norit SX plus, Norit Americas Inc., TX, USA) and the conductive carbon materials with different ratio of carbon black (CB, Vulcan XC-72, Cabot co., USA) and rGO (Table 2). 1 mL of 10% PVDF solution was added to the catalyst mixture, which was rigorously mixed by using a stainless steel poly spoon (HA.HSN, Hammacher, Germany). A catalytic dough was pasted on a stainless-steel mesh (60 mesh, SUS 304, total area of 11.3 cm^2, projected area of 7 cm^2 in the MFC) by using a stainless steel poly spoon. The stainless steel mesh pasted with the catalytic layer was placed in deionized water for 15 min to allow phase inversion to occur. After 15 min, it was taken out of the water bath was dried at room temperature for at least 6 h before use [6]. Thicknesses of five points in each cathode was measured by using a vernier caliper (BD293-025, BLUETEC, South Korea) and an average thickness of each cathode was calculated (Fig. 9-A).

Table 2
The mass and composition ratios of AC, CB and rGO in the catalyst layer of each cathode.

Cathode	Mass (mg)				Ratio (%)			
	AC	CB	rGO	Total	AC	CB	rGO	Total
rGO0	300	30	0	330	90.9	9.1	0	100
rGO5	300	25	5	330	90.9	7.6	1.5	100
rGO15	300	15	15	330	90.9	4.5	4.5	100
rGO30	300	0	30	330	90.9	0	9.1	100

As an anode electrode, a carbon fiber brush anode (2.5 cm in diameter and 2.5 cm in length) was made with carbon fibers (T700, TORAYCA, Japan) and two titanium wires (Length: 7 cm, 17 gauge; #2 grade; Seoul Titanium, South Korea) [23]. The brush anode was heat-treated at 450 °C in a normal air condition for 30 min in a furnace (FX/FHX, DAIHAN, South Korea) before use [24]. Two brush anodes were fabricated. They were inoculated and enriched in the operating MFC condition, and used for the cathode tests.

2.4. MFC construction and operation

Duplicate single-chamber MFCs were constructed as previously described [23,25]. It was made by drilling 28-ml cylindrical bed volume (4 cm length and 3 cm diameter) in a cubic polycarbonate block. A cathode electrode was placed in the cubic reactor, having

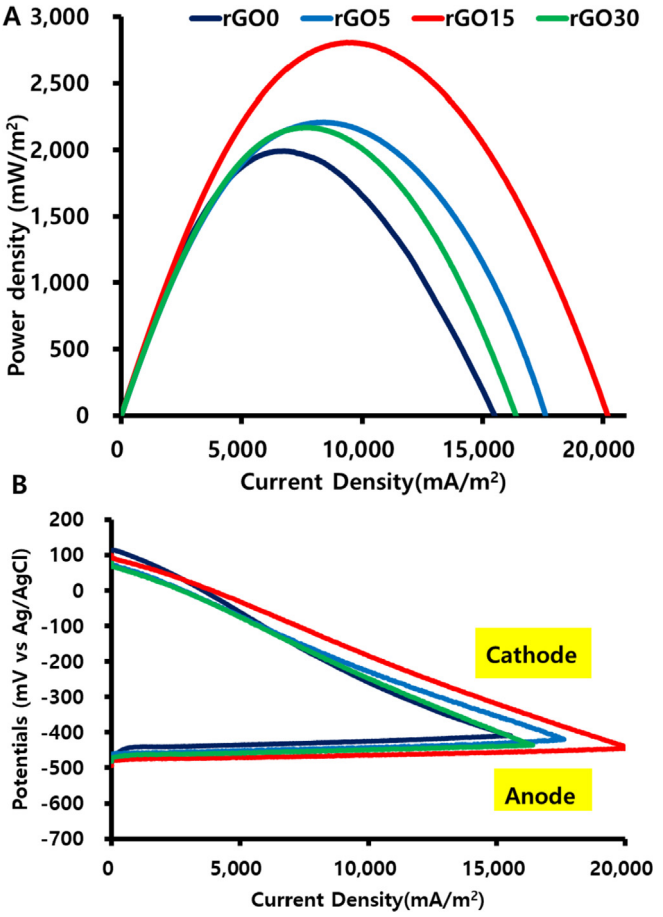

Fig. 1. Power density curves (A) and polarization curves for anodes and cathodes (B) of the MFCs with different cathodes. IV polarization test was performed with a scan rate of 1 mV/s.

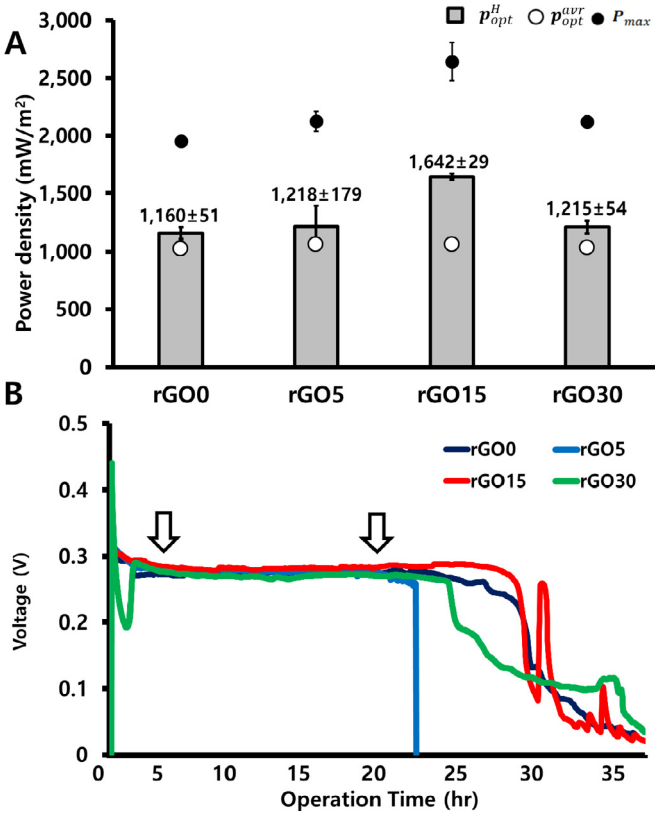

Fig. 2. Power density at optimal resistance(A) and MFC voltage profile(B). p_{opt}^{avr} is average power density at optimum resistance, p_{opt}^{H} is the highest power density at optimum resistance and p_{max} is measurement maximum power density in IV polarization measurement(A). And arrow means stable voltage production range during 1 batch cycle.

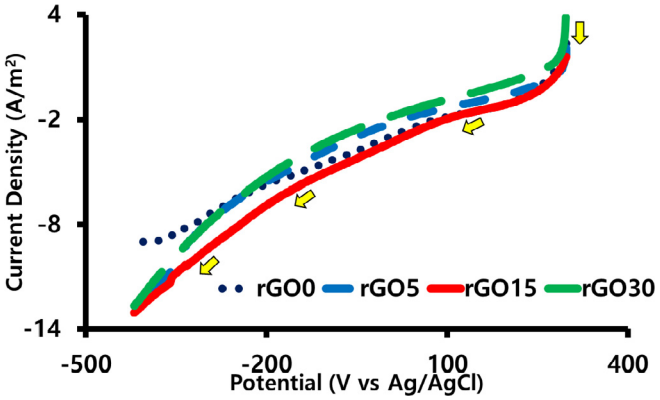

Fig. 3. Cathodic LSV measured in the abiotic cell with a scan rate of 0.1 mV/s.

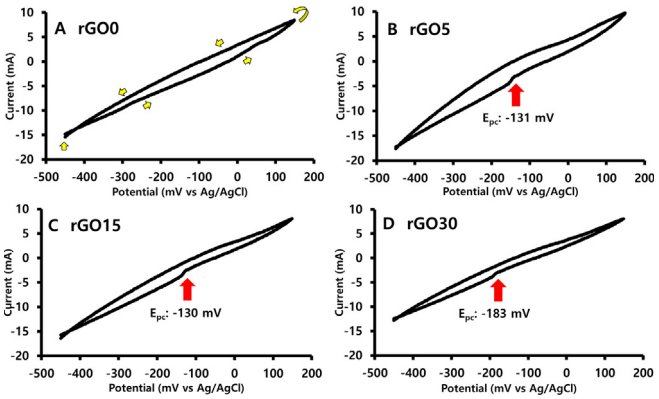

Fig. 4. Cathodic CV measured in the MFCs with a scan rate of 10 mV/s for rGO0 (A), rGO5 (B), rGO15 (C) and rGO30 (D). Yellow arrows indicate scanning direction and red arrows indicate reduction reaction peaks. In the rGO0 sample, reduction peak was not detected.

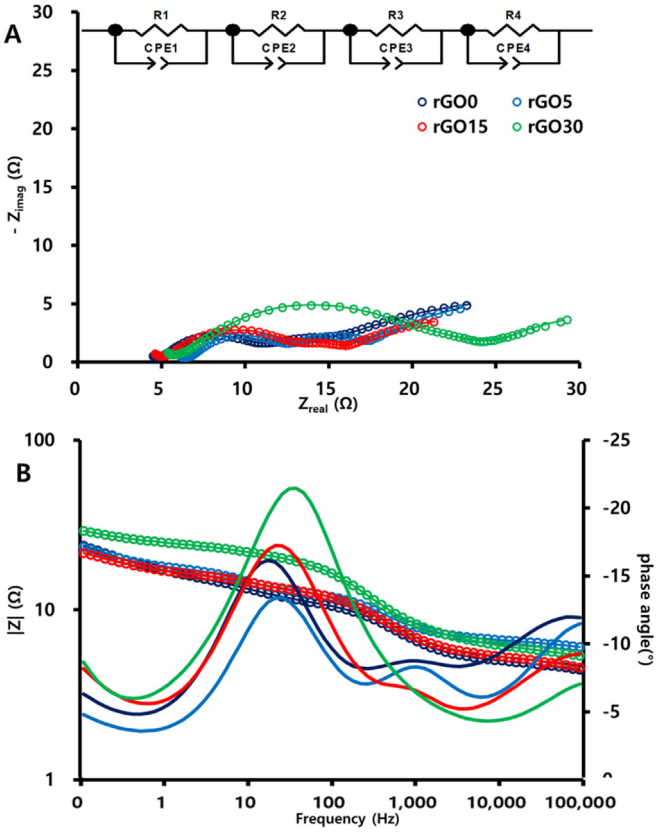

Fig. 5. Cathodic EIS results with Nyquist plot and the equivalent circuit fitting (A) and Bode plot (B). The dots are the impedance measurement result, and the lines are the equivalent circuit fittings. The inset (A) is the CPE circuit.

the projected area of 7 cm^2 in the medium. The titanium current collector of the brush anode was installed at a distance of 12 mm horizontally to the cathode to maximize power generation [23]. A titanium plate (10 × 25 mm, G2, Seoul titanium, South Korea) as a current collector was placed to the catalyst layer side of the cathode, and a nonwoven fabric (stationery store) was placed onto them as a separator to prevent the electrical short circuit between the anode and the cathode [26].

Two brush anodes used in this experiment were enriched for over one year in a 50-mM phosphate buffered saline (PBS) at a 100-Ω external resistor at a room temperature (30 °C). The PBS contained 2 g/L of sodium acetate hydrate (20 mM) and a 50-mM phosphate buffer solution (Na_2HPO_4, 4.33 g/L; NaH_2PO_4, 2.34 g/L; NH_4Cl, 0.31 g/L; KCl, 0.13 g/L; trace minerals, 10 mL/L; vitamin, 10 mL/L) [27]. All reactors were operated in a fed-batch mode in a constant temperature room (30 °C), and cell voltage was recorded at 1-min interval by using a multi-meter connected with a computer (3706A, Keithley Instrument, USA). When cell voltage dropped below 20 mV, the medium is replaced.

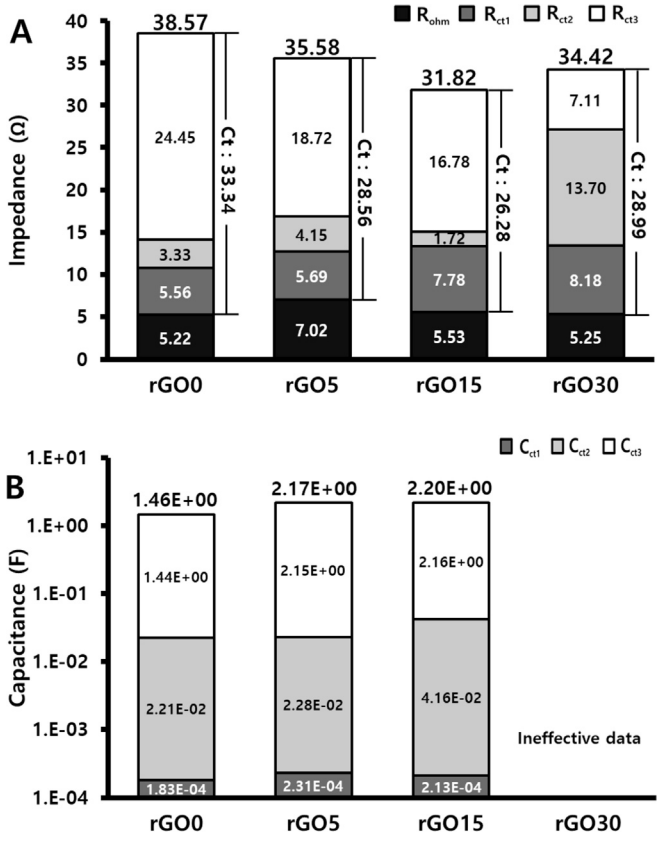

Fig. 6. Cathodic EIS results with impedance components (A) and capacitance (B) of the cathodes. R_{ohm} is ohmic impedance, R_{ct1}, R_{ct2} and Rct_3 are charge transfer impedance. The capacitance of rGO30 is invalid because capacitance value is regarded invalid if $T > 1$. rGO was cracked after MFC operation.

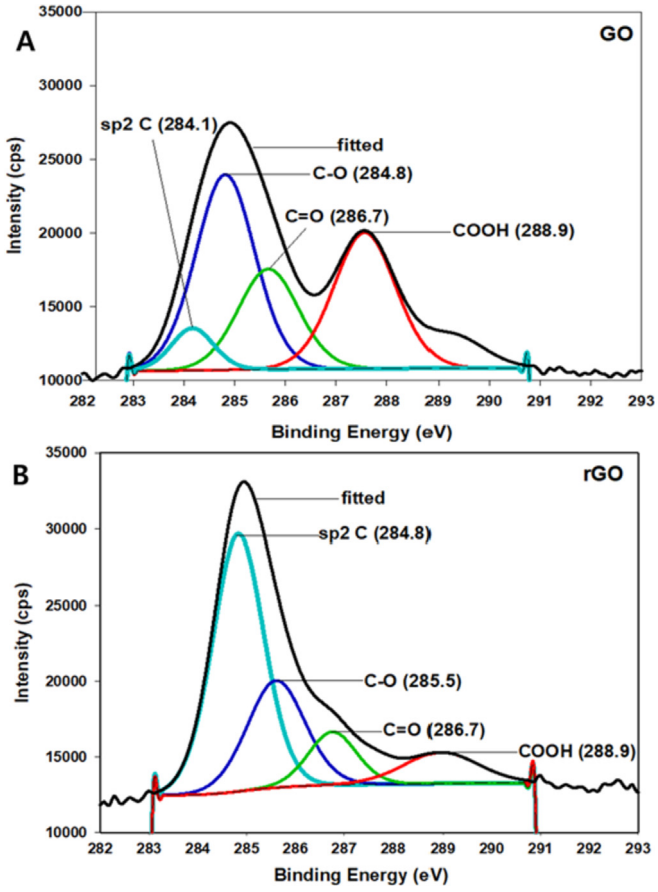

Fig. 8. The C 1s peaks of GO (A) and rGO (B) samples in the XPS spectra and their fittings.

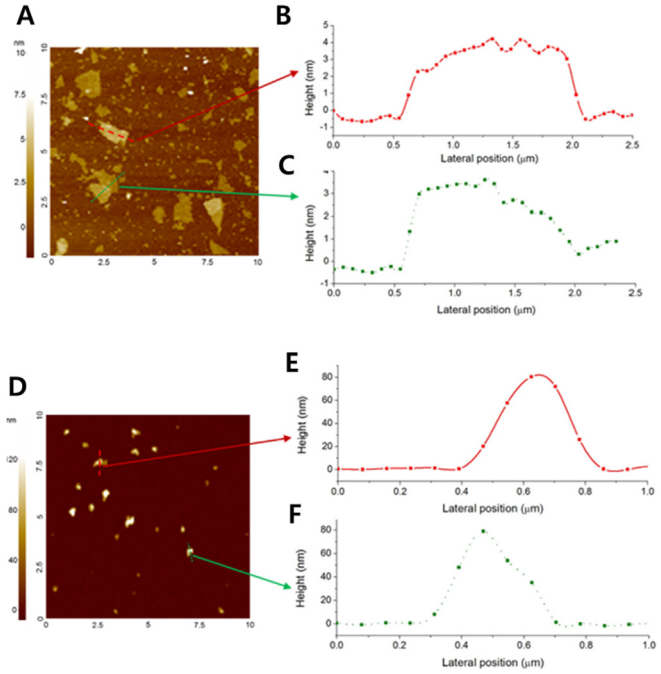

Fig. 7. AFM measurements of the rGO (A, B, C) and CB (D, E, F) sample. AFM image (10 μm × 10 μm area) (A, D), height profile along the lateral position of a designated particle with red (B, E) and green (C, F).

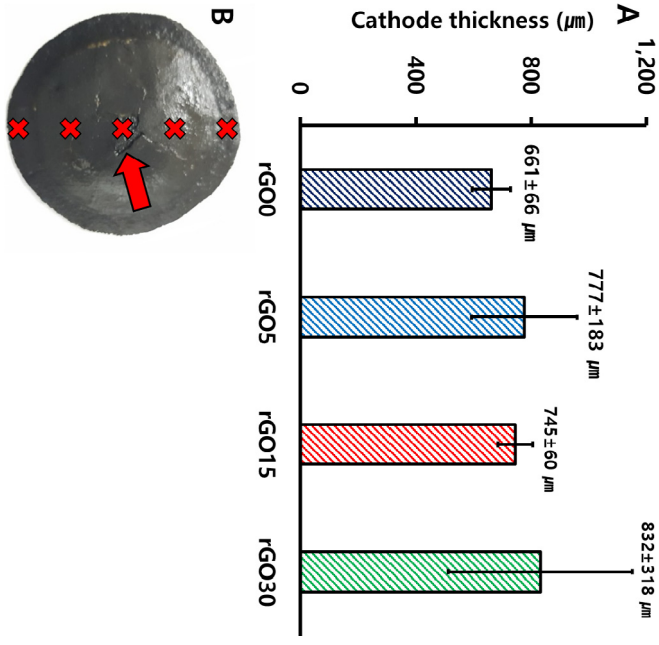

Fig. 9. Difference of Cathode thickness according to rGO contents. A was difference of cathode thickness of cathode, and B is a rGO30 cathode with a crack on the surface. And showed 5 thickness measuring point.

2.5. Electrochemical analysis

For IV polarization measurement, electrochemical impedance spectroscopy (EIS) and cathodic cyclic voltammetry (CV) in the full cell with the bioanode, the MFC was operated at 100-Ω external resistor for 1 h after medium change and then the sequences described below proceeded for each measurement. However, for the abiotic cathodic linear sweep voltammetry (LSV) and abiotic electrochemical measurement were performed without voltage stabilization due to the absence of the bioanode. All electrochemical measurements were performed in a constant temperature room (30 °C).

For electrochemical measurement of cathodic performance, LSV was performed by using a multichannel potentiostat (WMPG1000S, Wonatech, South Korea) in an abiotic cubic reactor (4 cm length, 3 cm diameter, single chamber) filled with the 50-mM PBS. A platinum wire (CHI115, CH Instruments, Germany) was used as the counter electrode, and an Ag/AgCl reference electrode (RE-1B, ALS, Japan; −0.209 V vs SHE) was placed close to a cathode. The potential scanned from +300 to −418 mV (vs. Ag/AgCl) at a scan rate of 0.1 mV/s [12].

For the IV polarization measurement, the MFC circuit was disconnected for 90 min and then connected to the potentiostat (ZIVE SP1, Wonatech, South Korea) in an open circuit mode for 30 min [25,28]. Then, a IV polarization test was conducted by decreasing the MFC voltage from open circuit voltage (OCV) to 0 V with the scan rate of 1 mV/s [23,28].

The cathodic CV were performed in three-electrode system in the MFC condition with the bioanode. The scan rate was 10 mV/s and cathodic potential range for CV was from −450 to 150 mV (vs Ag/AgCl), a cathode potential range in the cathodic polarization curves [29].

The potentiostatic cathodic EIS was performed in a three electrode system as previously described [23,28]. The MFC was poised at the cathode optimal potential for 30 min to make it produce a stable current. Impedance for each cathode was measured at its cathode optimal potential with the following conditions: amplitude 10 mV, 10^5 - 10^{-2} Hz of the frequency range, 10 points/decade of data acquisition [30,31].

Capacitance for each charge transfer step was calculated as,

$$C = \left[TR^{(1-\alpha)}\right]^{1/\alpha},$$

where C is the capacitance (F), T is the admittance ($S \cdot s^{\alpha}$), R_{ct} is the charge transfer impedance (Ω), α is the nonideality constant (dimensionless), S is siemens (S) and s is second (s). T is an element independent of the EIS measurement frequency [30,32]. T and α have a valid range from 0 to 1. When T and α are out of the valid range, it is considered invalid and [32].

2.6. Calculation

Power density, p (mW/m^2) and current density, i (mA/m^2) were calculated based on the cathodic projected area by $p = (I \cdot V)/A$ and $i = I/A$, respectively, where I is current (mA), V is voltage (mV) and A is the cathode projected area (7 cm^2).

Power density at optimum resistance (p_{opt}) was defined as power density generated during the MFC operation at the optimum resistance. The average power density (p_{opt}^{avr}) and average current density (i_{opt}^{avr}) were calculated from in the stable voltage profile (~13 h) during the MFC operation at the optimum resistance.

Optimum external resistance was calculated as,

$$R_{opt} = \frac{V_{opt}}{I_{opt}} = \frac{p_{max}}{(I_{opt})^2},$$

where R_{opt} is optimal external resistance (Ω), V_{opt} is the optimum cell voltage (V), p_{max} is maximum power (W), and I_{opt} is optimal current (A). R_{opt}, V_{opt}, and I_{opt} are the factors associated with maximum power generation in an MFC.

The EIS results were fitted with an equivalent circuit containing four constant phase elements (the CPE circuit, Fig. 6) using ZView software (version 3.5b).

Electrode potential was measured with a Ag/AgCl reference electrode, and it can be converted in to the SHE potential by using SHE = Ag/AgCl +209 mV. All the potential values in this manuscript were written in the Ag/AgCl standard electrode scale.

2.7. Data representation

Duplicate cathodes were constructed for the four cases by varying a ratio of carbon black (CB) and reduced graphene oxide (rGO). The duplicate brush anodes were pre-enriched for over one year and they were installed in the duplicate MFCs. Each cathode was tested two times. Two representative data from each cathode in duplicate were averaged and presented in this manuscript.

3. Results

3.1. Power and current production

rGO15 produced higher power and current density in the MFC than any other cathodes (Fig. 1 and Table 3). rGO0 having no reduced graphene oxide showed the lowest performance. rGO15 produced a 35% higher maximum power density, 21% higher optimum current density and 10% higher maximum current density than those of rGO0. Maximum power density on average in the MFC was in the rGO15 (2642 mW/m^2), which is 19%, 25% and 35% higher than those of rGO5 (2214 mW/m^2), rGO30 (2120 mW/m^2) and rGO0 (1955 mW/m^2), respectively. Optimum current density was in the rGO15 (9175 mA/m^2), which is 21%, 21% and 32% higher than those of rGO30 (7549 mA/m^2), rGO0 (7532 mA/m^2) and rGO5 (6900 mA/m^2), respectively. Maximum current density was in the rGO15 (19,348 mA/m^2), which is 10%, 19% and 21% higher than those of rGO0 (17,565 mA/m^2), rGO30 (16,158 mA/m^2) and rGO5 (15,987 mA/m^2), respectively.

To provide more realistic and practical power density values, an MFC was operated at its optimum external resistor and its power density value during the operation was averaged (p_{opt}^{avr}). In the optimum resistance operation, rGO5 showed the best power and current production and rGO15 showed similar performance to rGO5. Average power densities were highest in rGO5 (1063 mW/m^2), followed by rGO15 (1061 mW/m^2), rGO30 (1034 mW/m^2) and rGO0 (1023 mW/m^2). Average current densities during the optimum resistance operation (i_{opt}^{avr}) were highest in rGO5 (3896 mA/m^2), followed by rGO15 (3840 mA/m^2), rGO0 (3821 mA/m^2) and rGO30 (3792 mA/m^2). The average voltage production during the optimum resistance operation (V_{opt}^{avr}) were 272 ± 6 mV for rGO5, 268 ± 6 mV for rGO15, 268 ± 28 mV for rGO30 and 264 ± 7 mV for rGO0.

3.2. Polarization resistance

Cathodic polarization resistance, internal resistance in the full cell and optimum external resistance for maximum power generation were lowest in the MFC with the rGO15 cathode (Fig. 1 and

Table 3
Electrochemical data calculated from IV polarization tests and batch tests of the MFC operated at 100 Ω (n = 2). Values in parentheses of polarization resistance means the percentage of the polarization resistance of each electrode to the total internal resistance.

	OCV (mV)	p_{max} (mW/m^2)	i_{max} (mA/m^2)	i_{opt} (mA/m^2)	p_{opt}^{avr} (mW/m^2)	i_{opt}^{avr} (mA/m^2)
rGO0	562 ± 15	1955 ± 39	17,565 ± 2034	7532 ± 332	1023 ± 56	3821 ± 106
rGO5	560 ± 2	2124 ± 85	15,987 ± 1631	6900 ± 1566	1063 ± 51	3896 ± 93
rGO15	569 ± 28	2642 ± 163	19,348 ± 863	9175 ± 213	1061 ± 20	3840 ± 91
rGO30	550 ± 8	2120 ± 50	16,158 ± 244	7549 ± 25	1034 ± 179	3792 ± 31
	E_{cat}^{opt} (mv)	E_{an}^{opt} (mv)	R_{opt}	R_{int}	R_{cat}	R_{an}
rGO0	−187 ± 45	−447 ± 22	49.5 ± 7.7	52.2 ± 12.1 (100%)	49.7 ± 11.6 (95.2 ± 0.2%)	2.5 ± 0.5 (4.7 ± 0.2%)
rGO5	−130 ± 78	−452 ± 7	73.0 ± 41.0	66.4 ± 36.5 (100%)	67.2 ± 34.7 (94.2 ± 0.6%)	4.2 ± 1.8 (5.7 ± 0.6%)
rGO15	−168 ± 5	−456 ± 10	45.0 ± 1.4	44.8 ± 0.2 (100%)	42.6 ± 0.1 (94.9 ± 0.3%)	2.2 ± 0.1 (5.0 ± 0.3)
rGO30	−169 ± 4	−451 ± 3	53.5 ± 0.7	51.8 ± 1.6 (100%)	49.0 ± 1.3 (94.5 ± 1.1%)	2.8 ± 0.3 (5.4 ± 1.2%)

OCV, open circuit voltage; p_{max}, maximum power density; i_{max}, maximum current density; i_{opt}, optimal current density; p_{opt}^{avr}, average power density at optimum resistance; i_{opt}^{avr}, average current density at optimum resistance; E_{cat}^{opt}, optimum cathode potential; E_{an}^{opt}, optimum anode potential; R_{opt}, optimal external resistance; R_{int}, internal resistance of a full cell; R_{cat}, cathodic polarization resistance; R_{an}, anodic polarization resistance.

Table 3). The lowest cathodic polarization resistance detected in rGO15 (42.6 Ω), comparing with rGO30 (49.0 Ω), rGO0 (49.7 Ω) and rGO5 (67.2 Ω). The ratio of cathodic polarization resistance to internal resistance was 94–95%. The internal resistances were 44.8 Ω for rGO15, 51.8 Ω for rGO30, 52.2 Ω for rGO0 and 66.4 Ω for rGO5. The optimum external resistance, producing a maximum power in an MFC, were 45.0 Ω for rGO15, 49.5 Ω for rGO0, 53.5 Ω for rGO30 and 73.0 Ω for rGO5. Optimum external resistance in each MFC condition with a different cathode was similar to its own internal resistance. The anodic polarization resistances were almost similar (2.2–4.2 Ω) among the four cathodic conditions, because the two brush anodes were used for the duplicate MFC tests. Cathodic polarization resistances accounts for ~95% in the total internal resistance, with the remaining part of anodic polarization resistance (~5%).

3.3. Cathodic LSV and CV

The cathodic LSV test showed that rGO15 displayed the best electrochemical performance among all the cathodes (Fig. 3 and Table 4). rGO15 had the highest current density of 13.06 A/m^2 in the negative direction, followed by rGO5 (13.01 A/m^2), rGO30 (12.69 A/m^2) and rGO0 (9.17 A/m^2) (Fig. 3). The CV test showed that rGO5 had the highest net current production of 26.68 mA, which was higher than rGO15 (24.50 mA), rGO0 (23.88 mA) and rGO30 (20.86 mA) (Fig. 4 and Table 4). Reduction peaks were detected at −183 mV in rGO30, -131 mV in rGO15 and -130 mV in rGO5. No reduction peak was detected in rGO0 [29].

3.4. Cathodic EIS

rGO15 had the lowest total cathodic impedance (Figs. 5 and 6, Table 5). Total cathodic impedance were 31.8 Ω for rGO15, 35.2 Ω for rGO30, 35.5 Ω for rGO5 and 38.5 Ω for rGO0. Cathodic ohmic impedance were 5.2 Ω for rGO0, 5.4 Ω for rGO30 5.5 Ω for rGO15 and 7.0 Ω for rGO5. Cathodic charge transfer impedances were 26.3 Ω for rGO15, 28.5 Ω for rGO5, 29.9 Ω for rGO30 and 33.3 Ω for rGO0. Charge transfer impedance accounts for 80–86% in the total cathodic impedance, with the remaining parts of ohmic impedances (14–20%).

rGO15 had the highest total cathodic capacitance and rGO5 showed a similar value. rGO0 had the lowest value (Fig. 6 and Table 5). The total capacitance of rGO5 (2.20 F) and rGO15 (2.17 F) were higher than that of rGO0 (1.45 F). The capacitance value of rGO30 was not reported because this value is invalid. If T is over 1, capacitance value is regarded invalid. In our data, T_{ct3} was 1.813 (Table 5).

Table 4
The highest current density (i_{LSV}^{H}) from the LSV tests and maximum current (I_{pa}), minimum current (I_{pc}) and current production ($\triangle I_p = I_{pa} - I_{pc}$) from the CV tests.

i_{LSV}^{H}(A/m^2)	rGO0	rGO5	rGO15	rGO30
	9.17	13.01	13.06	12.69
I_{pa} (mA)	8.45	9.71	8.04	8.08
I_{pc} (mA)	−15.44	−16.98	−16.46	−12.79
$\triangle I_p$ (mA)	23.89	26.69	24.50	20.87
Reduction peak (mV)	N/D	−131	−130	−183
Reduction current (mA)	N/D	−2.80	−2.80	−3.11

N/D: Not detected.

3.5. Characteristics of carbon materials

XPS was performed to determine the compositions and chemical states of GO and rGO. C 1s of the GO samples shows that peaks with different intensities centered at 284.1, 284.8, 286.7 and 288.9 eV were observed, corresponding to sp2 C, −C−O, −C═O and −COOH groups, respectively [33] (Fig. 8-A). However, in the rGO samples, the intensities of all the C 1s peaks binding to oxygen obviously decreased (Fig. 8-B), revealing that most of the oxygen containing species (C-O, C═O and COOH) were reduced. The increase of peak for rGO at 284.8 eV (sp2 C) in the C 1s region also suggests the formation of graphene.

The reduction of graphene oxide (rGO) particles were confirmed by the atomic component analysis (Table 6). After the reduction process with the H_2/Ar gas, the O/C ratio decreased from 1.05 to 0.12, indicating oxygen functional groups on the GO surface was reduced. AFM was utilized to characterize the morphological features of the samples (Fig. 7). The rGO sample had ~1000 nm in width and ~2 nm in heights, and the CB sample had ~200 nm in width and ~70 nm in heights. It showed that rGO was flatter and wider than CB. Conductivity for rGO and CB are 760 ± 140 mS/cm and 250 ± 45 mS/cm, respectively, showing the conductivity of rGO had about 5 times higher than that of CB.

As the rGO addition ration increased, the average thickness of the cathode also increased (Fig. 9-A, Table 5). Average thicknesses were 660 μm for rGO0, 745 μm for rGO15, 777 μm for rGO5 and 832 μm for rGO30. The average thickness of rGO0 (660 μm) was similar to the cathode thickness (600–700 μm) from the previous study [4,6]. The thickest rGO30 cracked the surface of the cathode after the MFC operation (Fig. 9-B).

Table 5
Cathodic EIS analysis results. R is the impedance (Ω), α is the nonideality constant (dimensionless) and T is the admittance ($S \cdot s^{\alpha}$), where S is siemens and s is second. Valid range of T and α is from 0 to 1. R_{ohm} is ohmic impedance, R_{ct1}, R_{ct2} and R_{ct3} are charge transfer impedance for each charge transfer detected in this test. Values in parentheses of impedance means the percentage of each impedance to the total impedance.

	rGO0	rGO5	rGO15	rGO30[a]
Cathode optimum potential (mV)	−152 ± 8	−117 ± 1	−142 ± 38	−136 ± 33
R_{ohm} (Ω)	5.22 (13.5%)	7.02 (19.7%)	5.53 (17.3%)	5.25 (15.3%)
R_{ct} (Ω)	33.34 (86.5%)	28.56 (80.3%)	26.28 (82.7%)	29.99 (84.7%)
$R_{ohm} + R_{ct}$ (Ω)	38.56 (100%)	35.58 (100%)	31.81 (100%)	35.24 (100%)
C (F)	1.46	2.17	2.20	2.70[b]
Thickness (μm)	661 ± 66	777 ± 183	745 ± 60	823 ± 318
R_{ct1} (Ω)	5.56	5.68	7.78	8.18
Cct_1 (F)	1.8E-04	2.3E-04	2.1E-04	3.5E-04
Tct_1	0.00078	0.00086	0.00107	0.00090
αct_1	0.78995	0.80196	0.74704	0.83843
R_{ct2} (Ω)	3.33	4.15	1.72	13.70
Cct_2 (F)	2.2E-02	2.3E-02	4.2E-02	1.7E-03
Tct_2	0.04186	0.03273	0.04652	0.01833
αct_2	0.75452	0.84700	0.95760	0.36503
R_{ct3} (Ω)	24.45	18.72	16.78	7.11
Cct_3 (F)	6.5E+00	2.2E+00	2.2E+00	2.7E+00
Tct_3	0.53295	0.55324	0.38835	1.81300[b]
αct_3	0.50634	0.63260	0.52206	0.86972

[a] rGO was cracked after MFC operation.
[b] The capacitance of rGO30 is invalid because capacitance value is regarded invalid if T > 1.

Table 6
Elementary analysis and particle size of GO and rGO particles.

	O/C ratio	Carbon (%)	Oxygen (%)	Hydrogen (%)	Nitrogen (%)	Lateral size (μm)	Thickness (nm)
GO (GO-V30-100)	1.0–1.1	43–47	47–52	≤2.0	N/D	≥30	~1.0–1.2
rGO (rGO-V30-100)	0.10–0.14	78–84	8–12	≤1.0	N/D	≥20	~1.0–1.4

4. Discussion

4.1. Graphene chemistry

Graphene has 2-dimensional crystalline sheet structure. In a carbon atom, its 4 valence electrons are available for chemical bonding. However, in graphene, one carbon atom is connected to the other three carbon atoms on the two-dimensional sheet, leaving one electron available in the z-axis. These free electrons are called pi electrons (π electrons) and are located above and below the graphene sheet, giving high conductivity. Among graphene-like materials, graphene oxide (GO) is obtained by treating 3-dimensional graphite with strong oxidizers, creating 2-dimensional a monolayer of graphite oxide. Due to the oxidizing process, GO attain oxygen atoms in its structure and they combine with pi-electrons of a carbon atom, reducing electrical conductivity of GO. Reduction process of GO removes oxygen groups, increasing electrical conductivity [34].

4.2. Chemical and physical properties of rGO, CB and AC

rGO have higher electrical conductivity than those of AC and CB. rGO can be added to a cathodic catalyst layer to increase its electrical conductivity. In carbonaceous catalyst components, carbon (C) accounts for 66.54% for activated carbon (AC), 78–84% for reduced graphene oxide (rGO) and 99.7% for carbon black (CB) [7,35] (Table 7). rGO had a lower carbon content than CB, however, rGO had 5 times higher electrical conductivity than CB due to its graphene-like structure and the reduced state with a lower oxygen content.

AC, CB, and rGO particles in a catalyst layer had different shape and size (Table 7). AC has a particle size ≤0.29 μm on average and has a graphite structure and different pore size [36]. CB are agglomerate particles with a particle size ranging from 0.8 to 8 μm [35,37]. However, rGO has a larger particle size (≤20 μm) than AC and CB and are a flatter and more homogeneous structure of 2-dimensional crystalline structure. Because of different particle size and shape of AC, CB, and rGO, they could be intercalated and pore size could be reduced in a catalyst layer. Because rGO has a flatter and longer shape and a monolayer with higher electrical conductivity, it could promote electron transfer in the catalyst layer.

4.3. The optimum ratio of rGO and CB

rGO15 cathode had a lower cathode thickness than the rGO5 cathode (rGO5; 777 μm, rGO15; 745μm) (Table 5, Fig. 9-A). The optimum amount of rGO could produce a denser catalytic layer and increase conductivity and connectivity in the catalyst layer. Possibly due to a more intercalation in the catalyst layer of rGO15, rGO15 could be thinner than rGO5. The catalyst layer of rGO30 consisted solely of AC and rGO. rGO30 was the thickest (832 μm) and had cracks on the surface after the MFC operation.

EIS results also show that the rGO addition improves cathode performance. Cathodic impedance of rGO15, rGO30 and rGO5 were lower than that of rGO0. In addition, rGO5 and rGO15 have higher capacitance than rGO0.

The CV showed rGO30 had a lowest reduction peak and a reduction peak was not detected in rGO0 (Fig. 4). A reduction peak was detected at −183 mV in rGO30, -131 mV in rGO15 and -130 mV in rGO5. As a reduction peak is lower, catalytic action is more active. In terms of reduction peak, rGO30 could be the best cathode, but its morphological crack hindered high power generation. rGO30 had the highest capacitance, but it was invalid data because the capacitance factor of rGO30 exceeded the effective range (Table 5).

Table 7
Elemental compositions and particle shapes of carbonaceous materials for the catalyst layer.

	Composition (%)				Size (μm)	Shape	Structure	Ref
	C	O	F	S				
AC (Norit SX plus)	66.54	–	32.64	–	≤0.29	Randomly porous	Graphite structure	[7]
CB (Vulcan XC-72)	99.7	–	–	0.3	0.8–8	–	Agglomerate	[35]
rGO (V30-100)	78–84	8–12	–	–	≤20	Flat particle[a]	2-d crystalline sheet	[34]

[a] Lateral size is less than 20 μm and thickness ranges from 1 to 1.4 nm.

In the CV measurement, rGO30 was the lowest reduction peak, but it did not lead to the improved performance because rGO30 had cracks on the cathode surface.

Due to morphological and electrochemical properties, rGO15 produced the highest maximum power density (2642 mW/m^2). Therefore, rGO15 is the optimal ratio of the catalyst layer. The optimum rGO addition improves the intercalation of the catalyst layer, has a suitable cathode thickness and a low internal resistance. And the improved the electrical conductivity of the catalyst layer and accelerate the electron transfer rate.

4.4. Cathodic reduction

In our test, a reduction peak in the CV measurement were similar to an optimum cathode potential, indicating that a reduction reaction of a cathode in CV is closely related with an optimum cathode potential where a maximum power density is produced in an MFC. In oxygen reduction reaction, a reduction potential for 4-electron transfer is 596 mV (vs Ag/AgCl) and a reduction potential for 2-electron transfer is 119 mV (vs Ag/AgCl) [38]. In our test, cathodic OCP was 113 mV for rGO0, 82 mV for rGO5, 99 mV for rGO15 and 77 mV for rGO30 (Fig. 1-B), suggesting that 2-electron reduction reaction was occurred in our cathodes.

4.5. Maximum power density and operational power density

In this study, the comparison of maximum power densities is fair and valid because the same scan rate (1 mV/s) was applied to the all cases. Experimental reproducibility is critical for pursuing true science. So, the IV polarization method was used in this study because it is much more reproducible than any other conventional method such as the external resistance change method. The main goal of our polarization tests is to compare the different cathodes in this study. For fair evaluation, we had a control, the cathode without rGO, which is a good reference to evaluate the effects of the rGO addition. So, the comparison of maximum power densities from the IV polarization tests is fair and valid.

To provide an actual maximum power density during the MFC operation, the operational power density was provided by averaging power densities during the optimum resistance operation (Table 3), which is more meaningful than the maximum power density from the power density curve. Maximum power densities from any polarization method are lower than operational power density. When anode microbial community adapts to a specific external resistance, MFC power becomes lower and stabilizes, which have already been observed and reported. It have been observed in the external resistance method [39,40], and in the IV polarization method with different scan rates of 0.1 mV/s [41], 0.2 mV/s [14,42], 0.5 mV/s [43] and 1 mV/s [8,9,23,25,28,44].

In actual operation, time staying on an optimum resistance in the actual MFC operation is much longer than in the polarization and power density curves. When the MFC is operated at one external resistor for a long time, power output gradually decreases over time. Because a maximum power density obtained from a power density curve is always higher than the actual power production, it is important to show power production at the optimum resistance.

4.6. Others

Material costs are $ 17.8/g for CB, $ 22.1/g for GO and $ 89.3/g for rGO, showing that rGO is the most expensive. In this case, cathode costs are $ 4.94/m^2 for rGO0, $ 8.19/m^2 for rGO5 and $ 14.69/m^2 for rGO15. For future research, finding a low cost material replacing rGO would be valuable.

In our study, the duplicate anodes were used. Anode and cathode are connected to each other in one cell. So, one has a great impact on the other, and vice versa. Anode resistance accounted for about 5% and cathode resistance accounted for a larger portion (Table 3), showing the fully-matured anodes in our test had a little on the MFC performance and differences of the MFC performance and electrochemistry were largely from cathodes.

In duplicate rGO30, a sudden voltage drop was observed in the beginning of the voltage production (Fig. 2-b). According to our lots of experiments in our lab, a sudden voltage drop was observed in the initial voltage production when there was a physical defect in the cathode or when the cathode was used for a long time.

5. Conclusion

In the AC-based cathode, carbon black (CB) is added as a conductive supporting material. To enhance the performance of the AC-based cathode, rGO replaced CB in the four different weight ratios of rGO to CB: rGO0 0:30; rGO5 5:25; rGO15 15:15; rGO30 30:0. rGO15 showed 35% higher maximum power density (2642 mW/m^2) than that of the rGO0 (1955 mW/m^2). During the optimum resistance operation, rGO5 showed the best power (1063 mW/m^2) and current (3896 mA/m^2) and rGO15 showed similar power (1061 mW/m^2) and current (3840 mA/m^2). rGO15 had the lowest cathodic polarization resistance (42.6 Ω) and the lowest total cathodic impedance (31.8 Ω). The total capacitance of rGO5 (2.20 F) and rGO15 (2.17 F) were higher than that of rGO0 (1.45 F). The cathodic LSV test showed that rGO15 had the highest current density of 13.06 A/m^2 in the negative direction. The CV test showed that rGO5 had the highest current production of 26.68 mA, which was higher than rGO15 (24.50 mA), rGO0 (23.88 mA) and rGO30 (20.86 mA). XPS revealed that most of the oxygen containing species were reduced. Atomic component analysis also showed that thermal reduction of GO decreased the O/C ratio from 1 to 0.1. AFM showed that rGO sample had ~1000 nm in width and ~2 nm in heights and the CB sample had ~200 nm in width and ~70 nm in heights, showing that rGO was flatter and wider than CB. Conductivity for rGO and CB were 760 ± 140 mS/cm and 250 ± 45 mS/cm, respectively, showing that rGO has 204% higher conductivity than that of CB. The rGO addition increased the average cathodic thickness: 660 μm for rGO0, 745 μm for rGO15, 777 μm for rGO5, and 832 μm for rGO30. Due to the flatter and wider shape of rGO comparing and ~200% higher electrical conductivity than carbon

black (CB), the addition of rGO improved cathodic performance, but the complete replacement of CB with rGO decreased the cathodic performance (rGO) due to the increased thickness and the morphological crack.

Disclamier

This article contains contents of the master thesis of Bonyoung Koo in 2017. This article also contains contests presented in an academic conference: 2017 ISBUT. The authors certify that there is no authorship dispute among the authors.

Acknowledgements

This research was supported by Basic Science Research Program through the National Research Foundation of Korea (NRF) funded by the Ministry of Education (NRF-2018R1D1A1B07050567), a research grant from Gwangju Green Environment Center in Ministry of Environment (17-04-10-14-12), and a research grant from Korea Electric Power Corporation through Korea Electrical Engineering and Science Research Institute (R15XA03-04).

References

[1] B.E. Logan, Exoelectrogenic bacteria that power microbial fuel cells, Nat. Rev. Microbiol. 7 (2009) 375–381.
[2] S.P. Jung, Practical implementation of microbial fuel cells for bioelectrochemical wastewater treatment, J. Kor. Soc. Urban Environ. 13 (2013) 93–100.
[3] T. Lee, A. Okamoto, S. Jung, R. Nakamura, J.R. Kim, K. Watanabe, K. Hashimoto, Microbial electrochemical technologies producing electricity and valuable chemicals from biodegradation of waste organic matters, in: N.C. Yates M, R. Miller, S. Pillai (Eds.), Manual of Environmental Microbiology, fourth ed., American Society of Microbiology, 2016, 5.1.4-1-5.1.4-14.
[4] H. Dong, H. Yu, X. Wang, Q. Zhou, J. Feng, A novel structure of scalable air-cathode without Nafion and Pt by rolling activated carbon and PTFE as catalyst layer in microbial fuel cells, Water Res. 46 (2012) 5777–5787.
[5] S.P. Jung, S. Pandit, Chapter 3.1 - important factors influencing microbial fuel cell performance, in: S.V. Mohan, S. Varjani, A. Pandey (Eds.), Microbial Electrochemical Technology, Elsevier, 2019, pp. 377–406.
[6] W. Yang, W. He, F. Zhang, M.A. Hickner, B.E. Logan, Single-step fabrication using a phase inversion method of poly (vinylidene fluoride)(PVDF) activated carbon air cathodes for microbial fuel cells, Environ. Sci. Technol. Lett. 1 (2014) 416–420.
[7] F. Zhang, S. Cheng, D. Pant, G. Van Bogaert, B.E. Logan, Power generation using an activated carbon and metal mesh cathode in a microbial fuel cell, Electrochem. Commun. 11 (2009) 2177–2179.
[8] B. Koo, H. Kang, T. Nam, E. Kim, S. Son, S.P. Jung, Performance enhancement of a microbial fuel cell by physico-chemical treatments of activated-carbon catalyst of an air cathode, J. Kor. Soc. Urban Environ. 16 (2016) 431–439.
[9] T. Nam, S. Son, E. Kim, H.V.H. Tran, B. Koo, H. Chai, J. Kim, S. Pandit, A. Gurung, S.-E. Oh, E.J. Kim, Y. Choi, S.P. Jung, Improved Structures of Stainless Steel Current Collector Increase Power Generation of Microbial Fuel Cells by Decreasing Cathodic Charge Transfer Impedance, Environmental Engineering Research, 2018.
[10] X. Wang, N. Gao, Q. Zhou, H. Dong, H. Yu, Y. Feng, Acidic and alkaline pretreatments of activated carbon and their effects on the performance of air-cathodes in microbial fuel cells, Bioresour. Technol. 144 (2013) 632–636.
[11] Z. Wang, Y. Liu, K. Li, D. Liu, T. Yang, J. Wang, J. Lu, The influence and mechanism of different acid treatment to activated carbon used as air-breathing cathode catalyst of microbial fuel cell, Electrochim. Acta (2017).
[12] W. Yang, B.E. Logan, Immobilization of a Metal–nitrogen–carbon Catalyst on Activated Carbon with Enhanced Cathode Performance in Microbial Fuel Cells, ChemSusChem, 2016.
[13] X. Zhang, D. Pant, F. Zhang, J. Liu, W. He, B.E. Logan, Long-term performance of chemically and physically modified activated carbons in air cathodes of microbial fuel cells, ChemElectroChem 1 (2014) 1859–1866.
[14] M. Kodali, S. Herrera, S. Kabir, A. Serov, C. Santoro, I. Ieropoulos, P. Atanassov, Enhancement of microbial fuel cell performance by introducing a nanocomposite cathode catalyst, Electrochim. Acta 265 (2018) 56–64.
[15] M. Kodali, C. Santoro, A. Serov, S. Kabir, K. Artyushkova, I. Matanovic, P. Atanassov, Air breathing cathodes for microbial fuel cell using Mn-, Fe-, Co- and Ni-containing platinum group metal-free catalysts, Electrochim. Acta 231 (2017) 115–124.
[16] X. Zhang, X. Xia, I. Ivanov, X. Huang, B.E. Logan, Enhanced activated carbon cathode performance for microbial fuel cell by blending carbon black, Environ. Sci. Technol. 48 (2014) 2075–2081.
[17] X. Zhang, Q. Wang, X. Xia, W. He, X. Huang, B.E. Logan, Addition of conductive particles to improve the performance of activated carbon air-cathodes in microbial fuel cells, Environ. Sci. Water Rese. Technol. 3 (2017) 806–810.
[18] A.K. Geim, K.S. Novoselov, The rise of graphene, Nat. Mater. 6 (2007) 183–191.
[19] B.H. Lee, J.-H. Lee, Y.H. Kahng, N. Kim, Y.J. Kim, J. Lee, T. Lee, K. Lee, Graphene-conducting polymer hybrid transparent electrodes for efficient organic optoelectronic devices, Adv. Funct. Mater. 24 (2014) 1847–1856.
[20] T. Kim, Y.H. Kahng, T. Lee, K. Lee, D.H. Kim, Graphene films show stable cell attachment and biocompatibility with electrogenic primary cardiac cells, Mol. Cell. 36 (2013) 577–582.
[21] Y.-H. Hwang, S.M. Lee, Y.J. Kim, Y.H. Kahng, K. Lee, A new approach of structural and chemical modification on graphene electrodes for high-performance supercapacitors, Carbon 100 (2016) 7–15.
[22] C. Santoro, M. Kodali, S. Kabir, F. Soavi, A. Serov, P. Atanassov, Three-dimensional graphene nanosheets as cathode catalysts in standard and supercapacitive microbial fuel cell, J. Power Sources 356 (2017) 371–380.
[23] H. Kang, J. Jeong, P.L. Gupta, S.P. Jung, Effects of brush-anode configurations on performance and electrochemistry of microbial fuel cells, Int. J. Hydrogen Energy 42 (2017) 27693–27700.
[24] Y. Feng, Q. Yang, X. Wang, B.E. Logan, Treatment of carbon fiber brush anodes for improving power generation in air–cathode microbial fuel cells, J. Power Sources 195 (2010) 1841–1844.
[25] T. Nam, S. Son, B. Koo, H.V. Hoa Tran, J.R. Kim, Y. Choi, S.P. Jung, Comparative evaluation of performance and electrochemistry of microbial fuel cells with different anode structures and materials, Int. J. Hydrogen Energy 42 (2017) 27677–27684.
[26] F. Zhang, J. Liu, I. Ivanov, M.C. Hatzell, W. Yang, Y. Ahn, B.E. Logan, Reference and counter electrode positions affect electrochemical characterization of bioanodes in different bioelectrochemical systems, Biotechnol. Bioeng. 111 (2014) 1931–1939.
[27] S. Jung, J.M. Regan, Comparison of anode bacterial communities and performance in microbial fuel cells with different electron donors, Appl. Microbiol. Biotechnol. 77 (2007) 393–402.
[28] B. Koo, S.P. Jung, Characterization of impedance and polarization of carbon-felt bioanodes and activated-carbon cathodes in a continuous-flow microbial fuel cell, J. Kor. Soc. Urban Environ. 18 (2018) 177–191.
[29] C. Feng, Y. Liu, Q. Li, Y. Che, N. Li, X. Wang, Quaternary ammonium compound in anolyte without functionalization accelerates the startup of bioelectrochemical systems using real wastewater, Electrochim. Acta 188 (2016) 801–808.
[30] S. Jung, M.M. Mench, J.M. Regan, Impedance characteristics and polarization behavior of a microbial fuel cell in response to short-term changes in medium pH, Environ. Sci. Technol. 45 (2011) 9069–9074.
[31] S. Jung, Impedance analysis of geobacter sulfurreducens PCA, shewanella oneidensis MR-1, and their coculture in bioeletrochemical systems, Int. J. Electrochem. Sci. 7 (2012) 11091–11100.
[32] M.E. Orazem, B. Tribollet, Electrochemical Impedance Spectroscopy, John Wiley & Sons, 2011.
[33] C. Punckt, F. Muckel, S. Wolff, I.A. Aksay, C.A. Chavarin, G. Bacher, W. Mertin, The effect of degree of reduction on the electrical properties of functionalized graphene sheets, Appl. Phys. Lett. 102 (2013), 023114.
[34] S. Pei, H.-M. Cheng, The reduction of graphene oxide, Carbon 50 (2012) 3210–3228.
[35] D. Pantea, H. Darmstadt, S. Kaliaguine, C. Roy, Electrical conductivity of conductive carbon blacks: influence of surface chemistry and topology, Appl. Surf. Sci. 217 (2003) 181–193.
[36] N. Chada, J. Romanos, R. Hilton, G. Suppes, J. Burress, P. Pfeifer, Activated Carbon Monoliths for Methane Storage, APS Meeting Abstracts, 2012.
[37] S. Wolff, M. Wang, in: J.B. Donnet, R.C. Bansal, M.J. Wang (Eds.), Carbon Black Science & Technology, 1993.
[38] B.E. Logan, B. Hamelers, R. Rozendal, U. Schröder, J. Keller, S. Freguia, P. Aelterman, W. Verstraete, K. Rabaey, Microbial fuel cells: methodology and technology, Environ. Sci. Technol. 40 (2006) 5181–5192.
[39] G. Mohanakrishna, I.M. Abu-Reesh, S. Kondaveeti, R.I. Al-Raoush, Z. He, Enhanced treatment of petroleum refinery wastewater by short-term applied voltage in single chamber microbial fuel cell, Bioresour. Technol. 253 (2018) 16–21.
[40] I. Gajda, J. Greenman, C. Santoro, A. Serov, C. Melhuish, P. Atanassov, I.A. Ieropoulos, Improved power and long term performance of microbial fuel cell with Fe-N-C catalyst in air-breathing cathode, Energy (Oxford, England) 144 (2018) 1073–1079.
[41] T. Lin, W. Ding, L. Sun, L. Wang, C.-G. Liu, H. Song, Engineered Shewanella oneidensis-reduced graphene oxide biohybrid with enhanced biosynthesis and transport of flavins enabled a highest bioelectricity output in microbial fuel cells, Nano Energy (2018).
[42] S. Chen, S.A. Patil, U. Schröder, A high-performance rotating graphite fiber brush air-cathode for microbial fuel cells, Appl. Energy 211 (2018) 1089–1094.
[43] S. Luo, Z. He, Ni-coated carbon fiber as an alternative cathode electrode material to improve cost efficiency of microbial fuel cells, Electrochim. Acta 222 (2016) 338–346.
[44] S.P. Jung, E. Kim, B. Koo, Effects of Wire-type and Mesh-type Anode Current Collectors on Performance and Electrochemistry of Microbial Fuel Cells, Chemosphere, 2018.